Journal of
Mechanics of Materials and Structures

REFINEMENT OF PLASTICITY THEORY FOR MODELING MONOTONIC AND CYCLIC LOADING PROCESSES

Dmitry Abashev and Valentin Bondar

Volume 15, No. 2

March 2020

msp

JOURNAL OF MECHANICS OF MATERIALS AND STRUCTURES
Vol. 15, No. 2, 2020
dx.doi.org/10.2140/jomms.2020.15.225

REFINEMENT OF PLASTICITY THEORY FOR MODELING MONOTONIC AND CYCLIC LOADING PROCESSES

DMITRY ABASHEV AND VALENTIN BONDAR

Experimental analysis of 12X18H10T stainless steel specimens subjected to strain-controlled cyclic loading that comprises sequential monotonic and cyclic loading under uniaxial tension-compression and standard temperature is used to identify some features and dissimilarities of isotropic and kinematic hardening processes that occur during monotonic and cyclic loading. In order to describe these features in terms of the plasticity theory (the Bondar model), which can be classified as a combined-hardening flow theory, plastic-strain redirection criterion and the memory surface concept are introduced in the plastic-strain tensor space so as to separate monotonic and cyclic strain. Evolution equations for isotropic and kinematic hardening processes are derived to describe the monotonic-to-cyclic and cyclic-to-monotonic evolutions in transients. The basic experiment used to determine the material functions consists of three stages: cyclic loading, monotonic loading and subsequent cyclic loading until fracture. The results of the basic experiment are fundamental to the proposed method for identifying the material functions. Basic-experiment results and the identification method are used to identify the room-temperature material functions of 12X18H10T stainless steel. The paper compares the computational analysis and the experimental analysis of stainless steel subjected to a strain-controlled fatigue test (loading) in five and seven stages monotonic and cyclic loading until fracture. It further compares the computational and experimental kinetics of stress-strain state throughout the deformation process. Changes in the amplitude and mean cycle stress during the cyclic stress stages are subsequently analyzed. These stages are characterized by hysteresis loop stabilization. Computational and experimental results fit reliably. The theory adequately describes the processes of how the kinetic, the range, and the middle cycle stress alter when subjecting a specimen to strain-controlled loading, which enables a more adequate description of stress-controlled loading, especially when loading is nonstationary and nonsymmetric.

1. Introduction

Nonstationary asymmetric cyclic strain is a deformation process which is a sequence of monotonic and cyclic loadings. It is a very complex problem to model such processes mathematically when subjecting a specimen to strain-controlled cyclic loading, even more so in case of stress-controlled loading. Besides, such loadings are associated with the hard-to-model hysteresis-loop ratcheting and stabilization. As for the assessment and prediction of the resource under nonstationary and asymmetric cyclic loading conditions, fatigue damage accumulation must be determined throughout the deformation process given the significant nonlinearity of such damage.

Mathematical modeling of strain and damage accumulation when subjecting a specimen to cyclic loading is mainly based on variants of plasticity theories belonging to the class of combined (isotropic

Keywords: monotonic and cyclic loading, plasticity theory, isotropic and anisotropic hardening, memory surface, basic experiment, identification method.

and kinematic) hardening plastic-flow theories as reviewed and analyzed in [Abdel-Karim 2009; 2010a; 2010b; 2011; Bari and Hassan 2002; Besson et al. 2010; Bondar 2013; 2004; Bondar and Danshin 2008; Bondar et al. 2014; 2015; 2016; 2017; 2018; Chaboche 2008; Chaboche et al. 2012; Chang et al. 2016; Hassan et al. 2008; Huang et al. 2014; Kan and Kang 2010; Kang and Kan 2007; Kapustin et al. 2015; Kim et al. 2013; Lee et al. 2014; 2017; Mitenkov et al. 2015; Muhammad et al. 2015; Qiao et al. 2015; Rahman et al. 2008; Smith et al. 2018; Taleb and Cailletaud 2011; Taleb et al. 2014; Volkov and Igumnov 2007; Volkov and Korotkikh 2008; Yu et al. 2015; Zecevic and Knezevic 2015; Zhu et al. 2014; 2017]. In this paper, such modeling is based on the Bondar model, a version of plasticity theory [Bondar 2013; 2004; Bondar and Danshin 2008; Bondar et al. 2014; 2015; 2016; 2017; 2018] which, as shown in [Bondar et al. 2017], is the most adequate version for describing cyclic loading-induced strain and fracture, as compared to the Korotkikh [Kapustin et al. 2015; Mitenkov et al. 2015; Volkov and Igumnov 2007; Volkov and Korotkikh 2008] or Chaboche [Besson et al. 2010; Chaboche 2008; Chaboche et al. 2012; Huang et al. 2014] models. This paper presents the basic equations of the Bondar model.

In order to identify the features of strain induced by nonstationary and asymmetric cyclic loading, strain-controlled loading is analyzed by subjecting 12X18H10T stainless steel specimens to tension-compression tests in a sequence of five stages: cyclic, monotonic, cyclic, monotonic, and cyclic loading until fracture. Analysis of the cyclic-to-monotonic and monotonic-to-cyclic transients shows the need to separate the monotonic and the cyclic deformation processes. To that end, a plastic-strain redirection criterion and the memory surface concept for separating the monotonic and cyclic deformation processes are introduced in the plastic-strain space. Evolution equations of isotropic and kinematic hardening parameters for monotonic and cyclic loading are further introduced in the Bondar plasticity theory equations.

Separation of the monotonic and cyclic strain is also a feature of the Korotkikh model [Volkov and Korotkikh 2008], where it is only used to describe the evolution of isotropic hardening. The memory surface in this model is constructed in the backstress deviator space while determining the maximum equivalent backstress value in the deformation process. In [Mitenkov et al. 2015; Volkov and Korotkikh 2008], the evolution of kinematic hardening in a plastic-strain deviator space is described by introducing a memory surface while determining the maximum equivalent plastic-strain amplitude in the deformation process. Volkov et al. [2018] used the same memory surface to describe the kinematic hardening evolution as in the case of isotropic hardening. All these approaches [Mitenkov et al. 2015; Volkov and Korotkikh 2008; Volkov et al. 2018] have one significant drawback: the resulting memory surface size can potentially decrease and increase at the end of the cycle, resulting in a chance of it either both monotonic or cyclic loading at the end of each cycle. Besides, the evolution equation for the maximum cyclic-loading equivalent backstress means that this value is always diminishing, although it should remain constant in a stabilized cycle. In conclusion, it should also be noted that there is no documented adequate rationale for the considered approaches [Mitenkov et al. 2015; Volkov and Korotkikh 2008; Volkov et al. 2018]. In [Chaboche et al. 1979; Nouailhas et al. 1985; Ohno 1982], the evolution of only isotropic hardening in plastic-strain deviator space is described by introducing a memory surface while determining the center and size of the memory surface in the deformation process.

Taking into account the identified features of monotonic and cyclic loading for the refined equations of the modified Bondar plasticity theory, this research has defined the basic experiment as well as the method for identifying the material functions. The material functions of 12H18N10T stainless steel at room temperature are obtained. This paper compares the computational analysis and experimental analysis of 12H18N10T stainless steel subjected to strain-controlled loading which is a sequence of monotonic and cyclic loadings. The kinetics of the stress-strain state is analyzed, and changes in the amplitude and mean stress of the cycle during the cyclic loading stages are taken into account.

2. Basic equations of the plasticity theory

A simplified version of the plasticity theory [Bondar et al. 2014; 2015; 2016; 2017; 2018], which is a partial version of the theory of inelasticity [Bondar 2013; 2004], is considered. This version is a single-surface combined-hardening flow theory. Its applicability is limited to small strains of initially isotropic metals at temperatures that entail no phase transformations, at such strain rates where dynamic and rheological effects are negligible. Kinetic equations of damage accumulation and use the work of Type II backstresses on the field of plastic strain as the value of energy spend to damage the material.

Below is a summary of the basic equations for this plasticity theory version.

$$\dot{\varepsilon}_{ij} = \dot{\varepsilon}^e_{ij} + \dot{\varepsilon}^p_{ij}, \tag{1}$$

$$\dot{\varepsilon}^e_{ij} = \tfrac{1}{E}[\dot{\sigma}_{ij} - \nu(3\dot{\sigma}_0\,\delta_{ij} - \dot{\sigma}_{ij})], \tag{2}$$

$$f(\sigma_{ij}) = \tfrac{3}{2}(s_{ij} - a_{ij})(s_{ij} - a_{ij}) - C^2 = 0, \tag{3}$$

$$\dot{C} = q_\varepsilon\,\dot{\varepsilon}^p_{eq}, \quad \dot{\varepsilon}^p_{eq*} = \left(\tfrac{2}{3}\dot{\varepsilon}^p_{ij}\,\dot{\varepsilon}^p_{ij}\right)^{1/2}, \tag{4}$$

$$\dot{a}_{ij} = \sum_{m=1}^{M} \dot{a}^{(m)}_{ij}, \tag{5}$$

$$\dot{a}^{(1)}_{ij} = \tfrac{2}{3}g^{(1)}\dot{\varepsilon}^p_{ij} + g^{(1)}_a\,a^{(1)}_{ij}\,\dot{\varepsilon}^p_{eq*}, \tag{6}$$

$$\dot{a}^{(2)}_{ij} = \tfrac{2}{3}g^{(2)}\,\dot{\varepsilon}^p_{ij} + g^{(2)}_a\,a^{(2)}_{ij}\,\dot{\varepsilon}^p_{eq*}, \tag{7}$$

$$\dot{a}^{(m)}_{ij} = \tfrac{2}{3}g^{(m)}\,\dot{\varepsilon}^p_{ij} \quad (m = 3, \ldots, M), \tag{8}$$

$$\dot{\varepsilon}^p_{ij} = \frac{\partial f}{\partial \sigma_{ij}}\lambda = \frac{3}{2}\frac{s^*_{ij}}{\sigma^*_{eq}}\dot{\varepsilon}^p_{eq*}, \quad s^*_{ij} = s_{ij} - a_{ij}, \quad \sigma^*_{eq} = \left(\tfrac{3}{2}s^*_{ij}\,s^*_{ij}\right)^{1/2}, \tag{9}$$

$$\dot{\varepsilon}^p_{eq*} = \frac{1}{E_*}\frac{3}{2}\frac{s^*_{ij}\,\dot{\sigma}_{ij}}{\sigma^*_{eq}}, \quad E_* = q_\varepsilon\sum_{m=1}^{M} g^{(m)} + \sum_{m=1}^{2} g^{(m)}_a\,a^{(m)*}_{eq}, \quad a^{(m)*}_{eq} = \frac{3}{2}\frac{s^*_{ij}\,a^{(m)}_{ij}}{\sigma^*_{eq}}, \tag{10}$$

$$\dot{\varepsilon}^p_{eq*} = \frac{1}{E_* + 3G}3G\frac{s^*_{ij}\,\dot{\varepsilon}_{ij}}{\sigma^*_{eq}}, \quad G = \frac{E}{2(1+\nu)}, \tag{11}$$

$$\sigma^*_{eq} < C \cup \dot{\varepsilon}^p_{eq*} \le 0 - \text{elasticity}, \quad \sigma^*_{eq} = C \cap \dot{\varepsilon}^p_{eq*} > 0 - \text{elastoplasticity}, \tag{12}$$

$$\dot{\omega} = \alpha\omega^{(\alpha-1)/\alpha}\,\frac{a^{(2)}_{ij}\,\dot{\varepsilon}^p_{ij}}{W_a}, \quad \alpha = \left(\frac{\sigma^{(2)}_a}{a^{(2)}_{eq}}\right)^{n_\alpha}, \quad a^{(2)}_{eq} = \left(\tfrac{3}{2}a^{(2)}_{ij}\,a^{(2)}_{ij}\right)^{1/2}. \tag{13}$$

Here, $\dot{\varepsilon}_{ij}$, $\dot{\varepsilon}^e_{ij}$, $\dot{\varepsilon}^p_{ij}$ are the total, elastic, and plastic strain rate tensors; σ_{ij}, s_{ij}, s^*_{ij}, a_{ij} are the stress tensor, stress deviator, active-stress, and backstress; ε^p_{eq*} is the accumulated plastic strain; ω is the damage; E, ν

are Young's modulus and Poisson's ratio; C is the radius (size) of the yield surface; $a_{ij}^{(1)}$, $a_{ij}^{(2)}$, $a_{ij}^{(m)}$ are Type I, Type II, and Type III backstress (yield surface center displacement deviator); q_ε, $g^{(m)}$, $g_a^{(m)}$ are the defining functions, the relationship whereof to the material functions is described below; W_a is the energy of destruction in case of proportional loading; n_α is the nonlinearity of the damage accumulation process (equals 1.5 for nearly any structural steel or alloy).

3. Experiments

The material used here is 12X18H10T stainless steel. The chemical composition and mechanical properties of the steel are tabulated in Table 1. The hot-rolled plate of the material was machined into a round, solid bar specimen for uniaxial monotonic and cyclic loading test. The configuration of the test specimen is illustrated in Figure 1. The uniaxial test was conducted using a Zwick Z100 electromechanic testing machine equipped with a computerized data acquisition system. An extensometer with 20 mm gage length was used to measure the strain. The specimens were tested under uniaxial strain cycling.

The experimental results are discussed in sections 4 and 6 by comparing them with the simulated results by the proposed model.

chemical composition				mechanical properties	
C	< 0.12	Si	< 0.8	Young's modulus (GPa)	198
Mn	< 2	Ni	9–11	Poisson's ratio	0.28
S	< 0.02	P	< 0.035	yield stress (MPa)	196
Cr	17–19	Cu	< 0.3	ultimate strength (MPa)	510
Ti	0.4–1.0	Fe	∼ 67	elongation (%)	40

Table 1. Chemical composition and mechanical properties of 12X18H10T stainless steel.

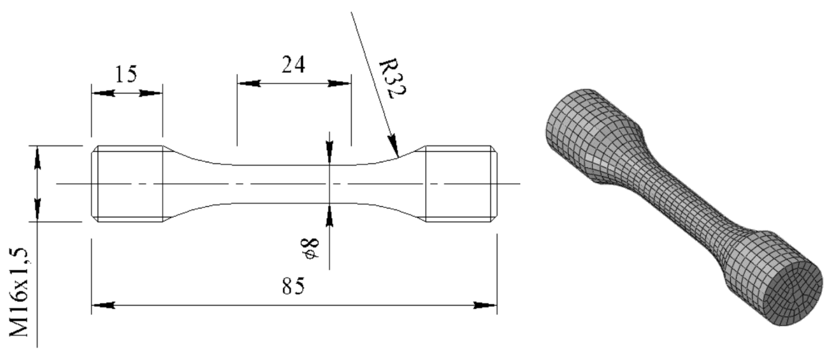

Figure 1. Configuration of the test specimen.

4. Monotonic and cyclic loading of 12X18H10T stainless steel

The paper presents the results of experimenting with 12X18H10T stainless steel subjected to uniaxial strain-controlled loading which is a sequence of monotonic and cyclic loading stages. The experiment consists of five loading stages:

- stage I involves cyclic loading at $\varepsilon_m^{(1)} = 0,\ \Delta\varepsilon^{(1)} = 0.016$ and $N^{(1)} = 20$ cycles;
- stage II involves monotonic tension test up to $\varepsilon^{(2)} = 0.05$;
- stage III involves cyclic loading at $\varepsilon_m^{(3)} = 0.05,\ \Delta\varepsilon^{(3)} = 0.012$ and $N^{(3)} = 200$ cycles;
- stage IV involves monotonic tension up to $\varepsilon^{(4)} = 0.1$;
- stage V involves cyclic loading at $\varepsilon_m^{(5)} = 0.1,\ \Delta\varepsilon^{(5)} = 0.012$ and $N^{(5)} = N_f$ cycles until fracture.

Here, $\varepsilon_m^{(i)}$ is the mean cycle strain; $\Delta\varepsilon^{(i)}$ is the cycle strain amplitude; $\varepsilon^{(i)}$ is the final monotonic strain; $N^{(i)}$ is the number of cycles.

Figure 2 shows the experimental diagram of 12X18H10T steel strain that covers all five loading stages. The cyclic diagrams of stages I, II, and III show the loops for the first cycle and the last cycle. Experimental results are analyzed below.

Cyclic deformation at stage I entails a cyclical hardening of 12X18H10T steel at the initial stage which slows down to insignificant levels; then the steel becomes virtually cyclically stable.

Stages III and V feature stabilization of the hysteresis loop. These stages are stabilization-wise identical, as if there was no prehistory of strain. Thus, the modulus $g^{(1)}$, which is part of the Type I backstress evolution equation and is necessary for loop stabilization, must have the same initial value $g^{(1)} = g_0^{(1)}$. That said, during monotonic postcyclic loading, when $g^{(1)}$ is reduced to nearly zero, the modulus $g^{(1)}$ must quickly return to its initial value $g_0^{(1)}$.

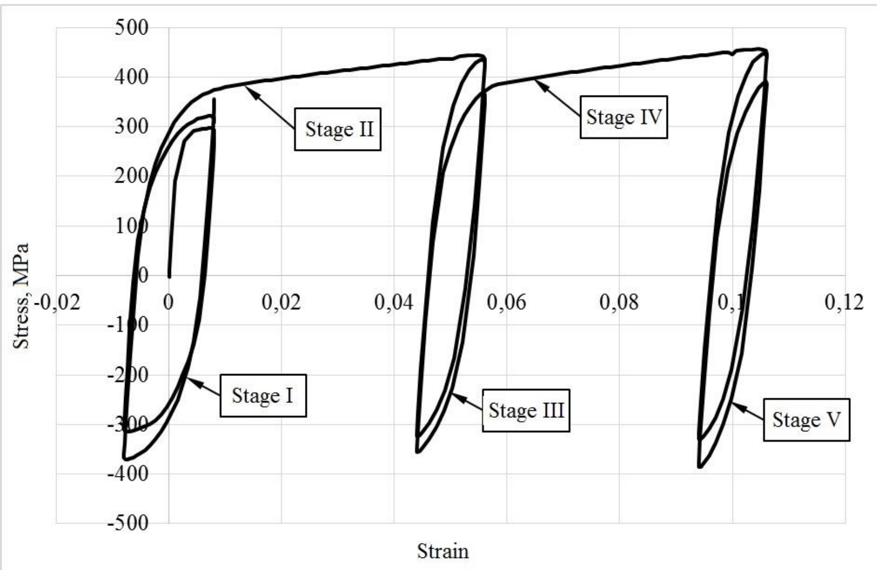

Figure 2. Stress-strain diagram of 12X18H10T steel.

Hardening is constant at stages II and IV of monotonic loading. Here, hardening is determined by the modulus $g_0^{(1)}$, and to a lesser extent by the modulus of monotonic isotropic hardening.

Thus, the behavior of the modulus $g^{(1)}$ that describes the kinematic hardening, and therefore the behavior of the isotropic hardening parameters, will to a significant extent depend on whether the strain is cyclic or monotonic.

Memory surface that limits the cyclic deformation area is introduced in the plastic-strain tensor space ε_{ij}^{p} in order to separate monotonic and cyclic strain. The surface is determined by the position of its center ξ_{ij} and its radius (size) C_ε. To compute the center and size of the surface, two plastic-strain tensors $\varepsilon_{ij}^{p(1)}$ and $\varepsilon_{ij}^{p(2)}$ are introduced to define the surface boundaries. These variables are zero as strain begins. The displacement and size of the memory surface are determined at the time plastic-strain is redirected. The following condition is assumed as the redirection criterion:

$$\dot{\varepsilon}_{ij(t-0)}^{p}\,\dot{\varepsilon}_{ij(t)}^{p} < 0, \tag{14}$$

where $\dot{\varepsilon}_{ij(t)}^{p}$ is the current plastic-strain rate tensor; $\dot{\varepsilon}_{ij(t-0)}^{p}$ is the plastic-strain rate tensor at the preceding time point.

At this moment, the change in the boundaries, center, and size of the yield surface is described based on the following relationships:

$$\varepsilon_{ij}^{p(2)} = \varepsilon_{ij}^{p(1)}, \tag{15}$$

$$\varepsilon_{ij}^{p(1)} = \varepsilon_{ij}^{p}, \tag{16}$$

$$\xi_{ij} = \frac{\varepsilon_{ij}^{p(1)} + \varepsilon_{ij}^{p(2)}}{2}, \tag{17}$$

$$C_\varepsilon = \left[\frac{2}{3}\left(\frac{\varepsilon_{ij}^{p(1)} - \varepsilon_{ij}^{p(2)}}{2}\right)\left(\frac{\varepsilon_{ij}^{p(1)} - \varepsilon_{ij}^{p(2)}}{2}\right)\right]^{1/2}. \tag{18}$$

Then the condition of cyclic strain is the strain within the memory surface:

$$F\big(\varepsilon_{ij}^{p}\big) = \tfrac{2}{3}\big(\varepsilon_{ij}^{p} - \xi_{ij}\big)\big(\varepsilon_{ij}^{p} - \xi_{ij}\big) - C_\varepsilon^2 \le 0. \tag{19}$$

Outside the memory surface ($F(\varepsilon_{ij}^{p}) > 0$), the strain is monotonous.

Based on the above peculiarities of monotonic and cyclic loading, the following equations are derived for backstress defining functions:

$$g^{(1)} = E_a, \quad g^{(2)} = \beta^{(2)}\,\sigma_a^{(2)}, \quad g_a^{(2)} = -\beta^{(2)}, \tag{20}$$

$$g^{(m)} = \begin{cases} \beta^{(m)}\,\sigma_a^{(m)}, & \\ 0, & a_{eq}^{(m)} \ge \sigma_a^{(m)} \cap a_{ij}^{(m)}\,s_{ij}^{*} > 0, \end{cases} \quad a_{eq}^{(m)} = \big(\tfrac{3}{2} a_{ij}^{(m)}\,a_{ij}^{(m)}\big)^{1/2}, \quad (m = 3, \dots, M), \tag{21}$$

$$\dot{E}_a = \begin{cases} -K_E (E_a/E_{a0})^{n_E}\,\dot{\varepsilon}_{eq*}^{p}, & \text{cyclic loading } (F(\varepsilon_{ij}^{p}) \le 0), \\ M_E\big(\frac{E_{a0}-E_a}{E_{a0}}\big)\,\dot{\varepsilon}_{eq*}^{p}, & \text{monotonic loading } (F(\varepsilon_{ij}^{p}) > 0), \end{cases} \tag{22}$$

$$g_a^{(1)} = \begin{cases} \frac{1}{E_a}\frac{dE_a}{d\varepsilon_{eq*}^{p}} = -\frac{1}{E_a} K_E (E_a/E_{a0})^{n_E}, & \text{cyclic loading } (F(\varepsilon_{ij}^{p}) \le 0), \\ 0, & \text{monotonic loading } (F(\varepsilon_{ij}^{p}) > 0), \end{cases} \tag{23}$$

where E_{a0}, $\sigma_a^{(m)}$, $\beta^{(m)}$ are the moduli of kinematic hardening; K_E, n_E, M_E are the parameters of kinematic hardening when the material is subjected to cyclic and monotonic strains. All of these material functions need to be derived in order to describe backstresses.

The kinematic hardening modulus E_{a0} is found by the formula

$$E_{a0} = \frac{\sigma_m^{(3)}}{\varepsilon_m^{p(3)}}, \tag{24}$$

where $\sigma_m^{(3)}$ is the mean stress in the first stage III cycle; $\varepsilon_m^{p(3)}$ is the mean plastic strain at the first stage III cycle.

The moduli of kinematic hardening $\sigma_a^{(m)}$ and $\beta^{(m)}$ are found by processing the cyclic diagram of the last stage I semicycle as per the procedure described in [Bondar 2013; Bondar et al. 2018].

The kinematic hardening parameters K_E and n_E are found based on the results of the hysteresis loop stabilization at stages III and V. To that end, the dependence in the coordinates

$$Y_E = \ln\left[\frac{\sigma_m(N-1) - \sigma_m(N)}{2\Delta\varepsilon^p\, \varepsilon_m^p}\right], \tag{25}$$

$$X_E = \ln\left[\frac{\sigma_m(N)}{\varepsilon_m^p\, E_{a0}}\right], \tag{26}$$

is constructed, where N is the cycle number; $\sigma_m(N)$ is the mean stress of the Nth cycle; $\Delta\varepsilon^p$ is the plastic-strain amplitude; ε_m^p is the mean plastic strain. The dependence obtained is approximated by the linear function

$$Y_E = a_E X_E + b_E. \tag{27}$$

Thus

$$K_E = \exp(b_E), \quad n_E = a_E. \tag{28}$$

The parameter of kinematic hardening M_E of a specimen subjected to monotonic loading is determined from the considerations of restoring the parameter E_a from 0 to the value E_{a0}, whereby plastic strain changes under monotonic loading over ε_{st}^p. Thus, the parameter M_E shall be determined by the formula

$$M_E = \frac{E_{a0}}{\varepsilon_{st}^p}. \tag{29}$$

Having found the backstresses over the entire process from stage I to stage V, one can determine the behavior of the yield surface size (radius), i.e., the change in isotropic hardening in cyclic-to-monotonic and monotonic-to-cyclic strain transients. Figure 3 shows the change in the yield surface size (functional C) throughout the deformation process from stage I to stage V.

The dotted line in Figure 3 shows the function of isotropic hardening $C = C_p(p)$ induced by cyclic loading. Analysis of the results presented in Figure 2 shows that the transition from cyclic to monotonic strain (stages II and IV) is associated with an increase in the intensity of isotropic hardening, and the transition from monotonic to cyclic strain (stages III and V) is associated with a slowdown in such isotropic hardening, as it tends to be isotropic $C = C_p(p)$ when subjecting the specimen to cyclic strain.

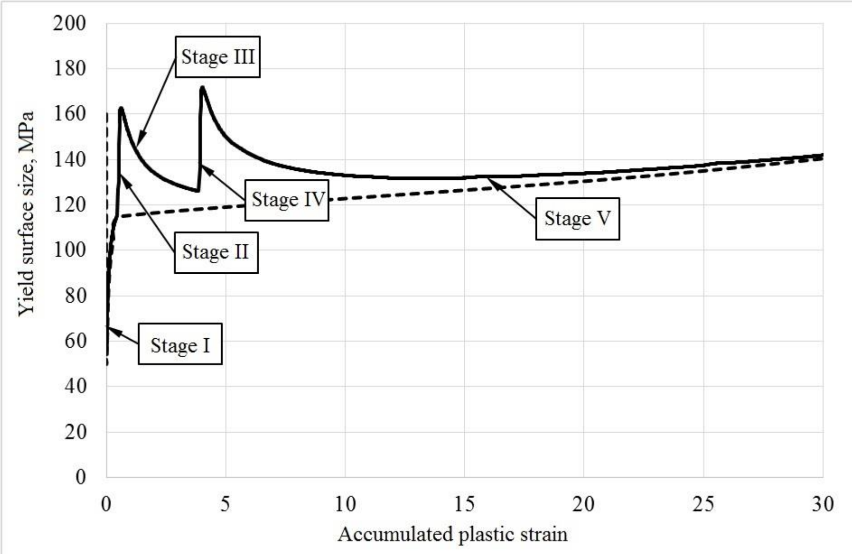

Figure 3. Cyclic and full yield surface size change.

Based on the above peculiarities of how isotropic hardening is altered by cyclic or monotonic loading, the following dependence is assumed for the defining function of isotropic hardening:

$$q_\varepsilon = \begin{cases} \left[dC_p/d\varepsilon^p_{eq*} - K_C\left(\frac{C-C_p}{C_p}\right)^{n_C}\right], & \text{cyclic loading } \ (F(\varepsilon^p_{ij}) \le 0), \\ \left[dC_p/d\varepsilon^p_{eq*} + M_c\right], & \text{monotonic loading } \ (F(\varepsilon^p_{ij}) > 0). \end{cases} \tag{30}$$

Thus, to describe such isotropic hardening, the following material functions must be defined: $C_p(\varepsilon^p_{eq*})$, the function of isotropic hardening induced by cyclic loading; K_C, n_C, M_C — the moduli of isotropic hardening induced by cyclic and monotonic loading. These material functions are defined using the experimental results (see Figure 3).

The function of isotropic hardening induced by cyclic loading $C_p(\varepsilon^p_{eq*})$ is determined based on the surface-size changes at stages I, III, and V (see the dotted curve in Figure 3).

Cyclic-loading isotropic hardening parameters K_C and n_C are found from the results of decreasing the yield surface size at stages III and V. To that end, a dependence is constructed in the coordinates

$$Y_C = \ln\left[\frac{d(C_p - C)}{d\varepsilon^p_{eq*}}\right], \tag{31}$$

$$X_C = \ln\left[\frac{C - C_p}{C_p}\right]. \tag{32}$$

The dependence obtained is approximated by the linear function

$$Y = a_C X_C + b_C. \tag{33}$$

Thus

$$K_C = \exp(b_C), \quad n_C = a_C. \tag{34}$$

E (MPa)	$2 \cdot 10^5$	ν	0.3	E_{a0} (MPa)	1000	$\sigma_a^{(2)}$ (MPa)	140
$\beta^{(2)}$	400	K_E (MPa)	7000	n_E	3	M_E (MPa)	$5 \cdot 10^5$
K_C (MPa)	260	n_C	1.4	M_C (MPa)	600	$\sigma_a^{(3)}$ (MPa)	600
$\beta^{(3)}$	$2 \cdot 10^3$	$\sigma_a^{(4)}$ (MPa)	30	$\beta^{(4)}$	1000	$\sigma_a^{(5)}$ (MPa)	22
$\beta^{(5)}$	444	$\sigma_a^{(6)}$ (MPa)	8	$\beta^{(6)}$	250	$\sigma_a^{(7)}$ (MPa)	6
$\beta^{(7)}$	143	W_a (MJ/M^3)	2400	n_a	1.5		

Table 2. Material functions of 12X18H10T steel.

ε^p_{eq*}	0	0.0003	0.0006	0.0014	0.0045	0.006	0.01	0.025		
C_p (MPa)	165	150	140	110	70	55	50	65		
ε^p_{eq*}	0.01	0.15	0.3	0.45	0.6	1	8	25	45	65
C_p (MPa)	90	100	112	115	120	124	130	135	140	150

Table 3. Isotropic hardening function of 12X18H10T steel.

The parameter of isotropic hardening M_C induced by monotonic strain is found from the slope of the strain curve at stages II and IV using

$$M_C = \frac{d\sigma}{d\varepsilon^p} - E_{a0} - \frac{dC_p}{d\varepsilon^p}. \tag{35}$$

Definition of damage variables is given in [Bondar and Danshin 2008]. To define this variables by the results of only one experiment, n_α should be taken equal to 1.5 and W_a should be found correctly in order to calculate the number of cycles till failure in the experiment.

5. Material functions of 12X18H10T stainless steel

Material functions have been derived based on the results of the experiments in room-temperature with 12X18H10T stainless steel (see tables 2 and 3).

The isotropic hardening function $C_p(\varepsilon^p_{eq*})$ is set forth either in analytical form or as a table with linear cuterpolation between points.

6. Verification of the modified plasticity theory

To verify the modified plasticity theory, the researchers have computed the kinetics of the stress-strain state of 12X18H10T stainless steel subjected to strain-controlled cyclic and monotonic loading according to the five-stage program described in Section 4. Computation uses the material functions per Section 5. Figure 4 (top) shows the computed results and Figure 4 (bottom) the experimental results of the cyclic diagrams at stages I, III, V and the monotonous loading at stages II, IV. Variations in the stress range and middle cycle stress at stages I, III and V are shown in figures 5 and 6; in these figures, a comparison between computed (solid curves) and experimental (open circles) results is present. Experimental and computed cycles until fracture equal to 2700 and 2400 cycles, respectively.

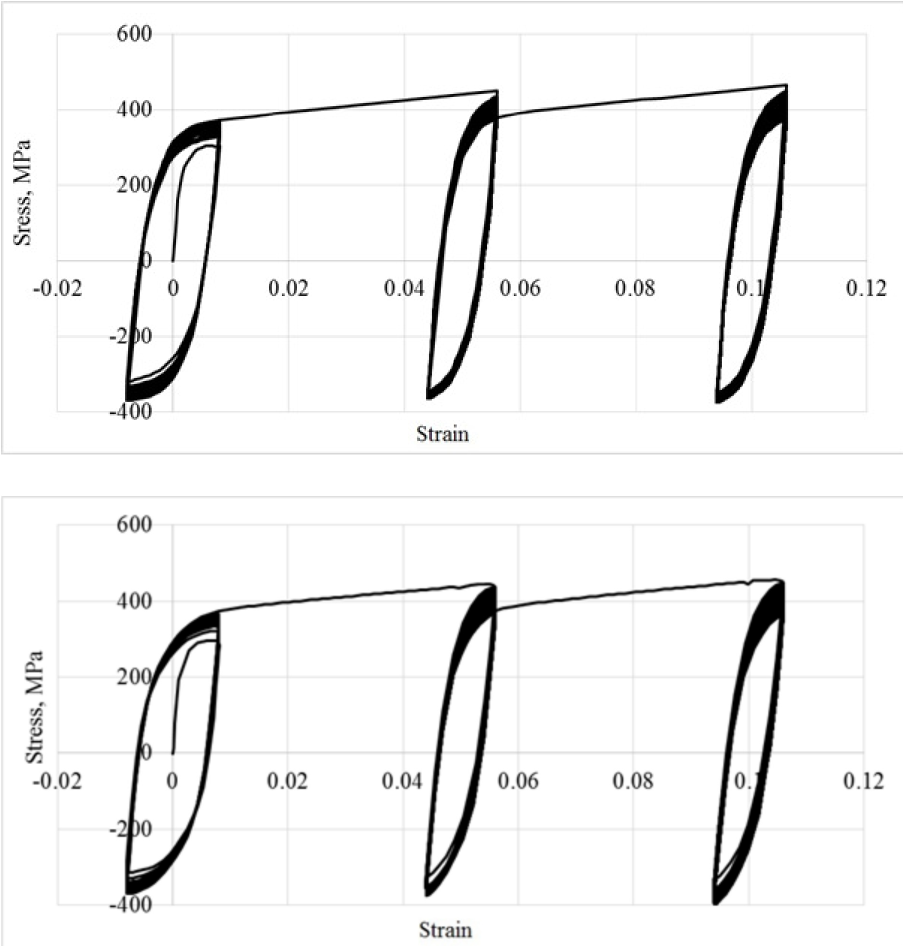

Figure 4. Cyclic diagram of five-stages experiment: calculated (top) and experimental (bottom).

To verify the modified plasticity theory, the researchers have computed the kinetics of the stress-strain state of 12X18H10T stainless steel subjected to strain-controlled cyclic and monotonic loading according to seven-stage program.

The experiment consists of seven loading stages:

- stage I involves cyclic loading at $\varepsilon_m^{(1)} = 0$, $\Delta\varepsilon^{(1)} = 0.002$ and $N^{(1)} = 500$ cycles;
- stage II involves cyclic loading at $\varepsilon_m^{(2)} = 0$, $\Delta\varepsilon^{(2)} = 0.012$ and $N^{(2)} = 500$ cycles;
- stage III involves cyclic loading at $\varepsilon_m^{(3)} = 0.008$, $\Delta\varepsilon^{(3)} = 0.008$ and $N^{(3)} = 500$ cycles;
- stage IV involves monotonic tension test up to $\varepsilon^{(4)} = 0.03$;
- stage V involves cyclic loading at $\varepsilon_m^{(5)} = 0.025$, $\Delta\varepsilon^{(5)} = 0.01$ and $N^{(5)} = 500$ cycles;
- stage VI involves monotonic tension test up to $\varepsilon^{(6)} = 0.05$;
- stage VII involves cyclic loading at $\varepsilon_m^{(7)} = 0.046$, $\Delta\varepsilon^{(7)} = 0.008$ and $N^{(7)} = N_f$ cycles until fracture.

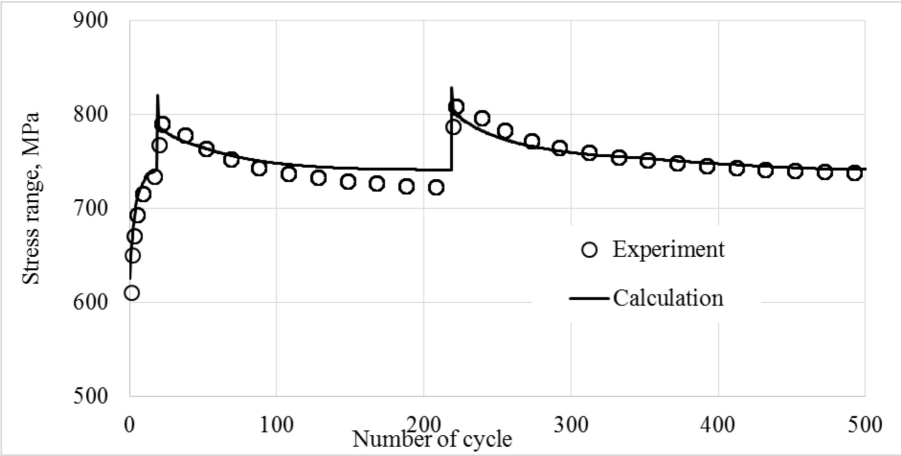

Figure 5. Calculated and experiment stress range in five-stages experiment.

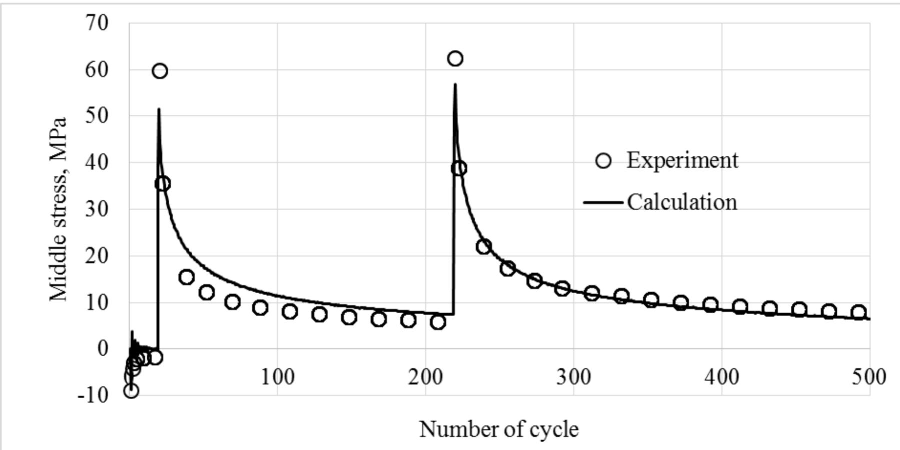

Figure 6. Calculated and experiment middle stress in five-stages experiment.

Computation uses the material functions per Section 5. Figure 7 (top) shows the computed results and Figure 7 (bottom) the experimental results of the cyclic diagram at stages I, II, III, V, VII and the monotonous loading at stages IV, VI. Variations in the stress range and middle cycle stress at stages I, II, III, V and VII are shown in figures 8 and 9; in these figures, a comparison of the computed (solid curves) and experimental (open circles) results is present.

Experimental and computed cycles until fracture equal to 6900 and 7600 cycles, respectively.

7. Conclusions

Analysis of the stainless-steel experiments leads to a conclusion that the processes of isotropic and kinematic hardening vary significantly depending on whether the strain is monotonic or cyclic. Monotonic-to-cyclic and cyclic-to-monotonic strain transitions are associated with hardening transients.

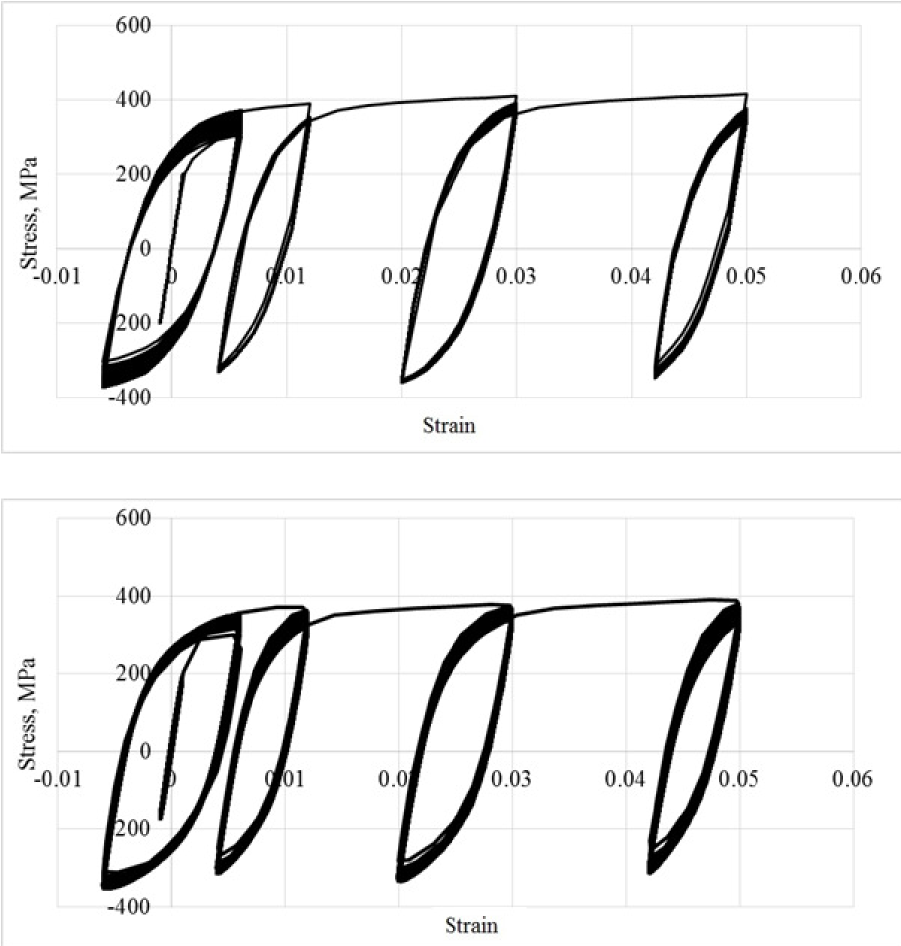

Figure 7. Cyclic diagram of seven-stages experiment: calculated (top) and experimental (bottom).

In the light of the identified features of monotonic and cyclic loading, the equations of the plasticity theory have been refined. The researchers have defined the basic experiment, derived the material-function identification method, and obtained such material functions for 12X18H10T stainless steel at room temperature.

The paper compares the results of computational and experimental studies of 12X18H10T stainless steel subjected to strain-controlled loading, a process consisting in a sequence of monotonic and cyclic loadings. The stress-strain state kinetics has been analyzed. Changes in the stress range and middle stress of the cycle during cyclic loading have been dwelled upon. Computational and experimental results fit reliably.

The theory adequately describes the processes of how the kinetics, the stress ranges, and the middle cycle stress alter when subjecting a specimen to strain-controlled loading; this enables a more adequate description of stress-controlled loading, especially when loading is nonstationary and nonsymmetric.

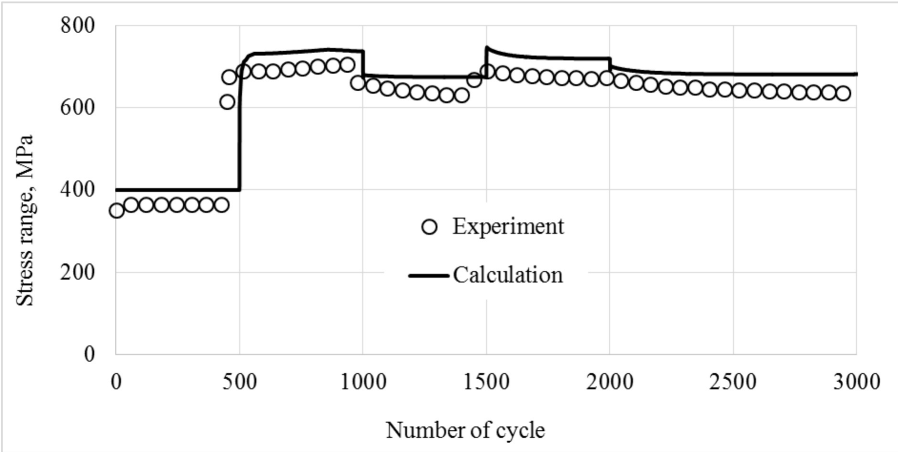

Figure 8. Calculated and experiment stress range in seven-stages experiment.

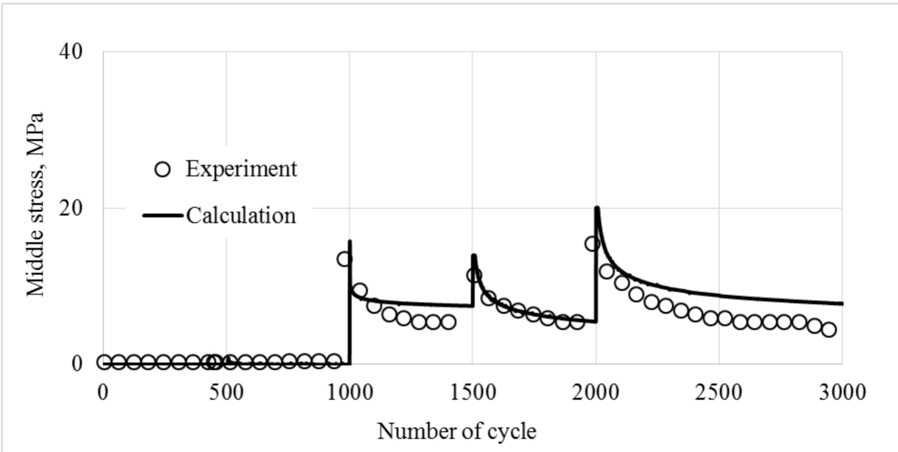

Figure 9. Calculated and experiment middle stress in seven-stages experiment.

References

[Abdel-Karim 2009] M. Abdel-Karim, "Modified kinematic hardening rules for simulations of ratchetting", *Int. J. Plast.* **25**:8 (2009), 1560–1587.

[Abdel-Karim 2010a] M. Abdel-Karim, "An evaluation for several kinematic hardening rules on prediction of multiaxial stress-controlled ratchetting", *Int. J. Plast.* **26**:5 (2010), 711–730.

[Abdel-Karim 2010b] M. Abdel-Karim, "An extension for the Ohno–Wang kinematic hardening rules to incorporate isotropic hardening", *Int. J. Press. Vessels Pip.* **87**:4 (2010), 170–176.

[Abdel-Karim 2011] M. Abdel-Karim, "Effect of elastic modulus variation during plastic deformation on uniaxial and multiaxial ratchetting simulations", *Eur. J. Mech. A Solids* **30**:1 (2011), 11–21.

[Bari and Hassan 2002] S. Bari and T. Hassan, "An advancement in cyclic plasticity modeling for multiaxial ratcheting simulation", *Int. J. Plast.* **18**:7 (2002), 873–894.

[Besson et al. 2010] J. Besson, G. Cailletaud, J.-L. Chaboche, and S. Forest, *Non-linear mechanics of materials*, Springer, 2010.

[Bondar 2004] V. S. Bondar, Неупругост: варианты теории, Fizmatlit, Moscow, 2004.

[Bondar 2013] V. S. Bondar, *Inelasticity: variants of the theory*, Begell House, 2013.

[Bondar and Danshin 2008] V. S. Bondar and V. V. Danshin, Пластичность: пропорциональные и непропорциональные нагружения, Fizmatlit, Moscow, 2008.

[Bondar et al. 2014] V. S. Bondar, V. V. Danshin, and D. A. Makarov, "Математическое моделирование процессов деформирования и накопления повреждений при циклических нагружениях [Mathematical modelling of deformation and damage accumulation under cyclic loading]", *PNRPU Mech. Bull.* **2014**:2 (2014), 125–152.

[Bondar et al. 2015] V. S. Bondar, V. V. Danshin, and A. A. Kondratenko, "Вариант теории термопластичности [Version of the theory of thermoplasticity]", *PNRPU Mech. Bull.* **2015**:2 (2015), 21–35.

[Bondar et al. 2016] V. S. Bondar, V. V. Danshin, and A. A. Kondratenko, "Вариант теории термоязкоптастичности [Variant of thermoviscoplasticity theory]", *PNRPU Mech. Bull.* **2016**:1 (2016), 39–56.

[Bondar et al. 2017] V. S. Bondar, D. R. Abashev, and V. K. Petrov, "Сравнительный анализ вариантов теорий пластичности при циклических напружениях [Comparative analysis of variants of plasticity theories under cyclic loading]", *PNRPU Mech. Bull.* **2017**:2 (2017), 23–44.

[Bondar et al. 2018] V. S. Bondar, V. V. Danshin, D. L. Vu, and D. N. Duc, "Constitutive modeling of cyclic plasticity deformation and low-high-cycle fatigue of stainless steel 304 in uniaxial stress state", *Mech. Adv. Mater. Struct.* **25**:12 (2018), 1009–1017.

[Chaboche 2008] J.-L. Chaboche, "A review of some plasticity and viscoplasticity constitutive theories", *Int. J. Plast.* **24**:10 (2008), 1642–1693.

[Chaboche et al. 1979] J. L. Chaboche, K. D. Van, and G. Cordier, "Modelization of the strain memory effect on the cyclic hardening of 316 stainless steel", in *Transactions of the 5th International Conference on Structural Mechanics in Reactor Technology* (Berlin), 1979.

[Chaboche et al. 2012] J.-L. Chaboche, P. Kanouté, and F. Azzouz, "Cyclic inelastic constitutive equations and their impact on the fatigue life predictions", *Int. J. Plast.* **35** (2012), 44–66.

[Chang et al. 2016] K.-H. Chang, J.-T. Jeon, and C.-H. Lee, "Effects of residual stresses on the uniaxial ratcheting behavior of a girth-welded stainless steel pipe", *In. J. Steel Struct.* **16** (2016), 1381–1396.

[Hassan et al. 2008] T. Hassan, L. Taleb, and S. Krishna, "Influence of non-proportional loading on ratcheting responses and simulations by two recent cyclic plasticity models", *Int. J. Plast.* **24**:10 (2008), 1863–1889.

[Huang et al. 2014] Z. Y. Huang, J.-L. Chaboche, Q. Y. Wang, D. Wagner, and C. Bathias, "Effect of dynamic strain aging on isotropic hardening in low cycle fatigue for carbon manganese steel", *Mater. Sci. Eng. A* **589** (2014), 34–40.

[Kan and Kang 2010] Q. Kan and G. Kang, "Constitutive model for uniaxial transformation ratchetting of super-elastic NiTi shape memory alloy at room temperature", *Int. J. Plast.* **26**:3 (2010), 441–465.

[Kang and Kan 2007] G. Kang and Q. Kan, "Constitutive modeling for uniaxial time-dependent ratcheting of SS304 stainless steel", *Mech. Mater.* **39**:5 (2007), 488–499.

[Kapustin et al. 2015] S. A. Kapustin, Y. A. Churilov, and V. A. Gorohov, Моделирование нелинейного деформирования и разрушения конструкций в условиях многофакторных воздействий на основе МКЭ *[Simulation of nonlinear deformation and fracture of structures under conditions of multifactorial effects based on FEM]*, Izd-vo NGU, N. Novgorod, 2015.

[Kim et al. 2013] J. H. Kim, D. Kim, Y.-S. Lee, M.-G. Lee, K. Chung, H.-Y. Kim, and R. H. Wagonere, "A temperature-dependent elasto-plastic constitutive model for magnesium alloy AZ31 sheets", *Int. J. Plast.* **50** (2013), 66–93.

[Lee et al. 2014] C.-H. Lee, V. N. Van Do, and K.-H. Chang, "Analysis of uniaxial ratcheting behavior and cyclic mean stress relaxation of a duplex stainless steel", *Int. J. Plast.* **62** (2014), 17–33.

[Lee et al. 2017] J.-Y. Lee, M.-G. Lee, F. Barlat, and G. Bae, "Piecewise linear approximation of nonlinear unloading-reloading behaviors using a multi-surface approach", *Int. J. Plast.* **93** (2017), 112–136.

[Mitenkov et al. 2015] F. M. Mitenkov, I. A. Volkov, L. A. Igumnov, A. V. Kaplienko, I. G. Korotkikh, and V. A. Panov, Прикладная теория пластичности, Fizmatlit, Moscow, 2015.

[Muhammad et al. 2015] W. Muhammad, M. Mohammadi, J. Kang, and K. Mishra, R. K. Inal, "An elasto-plastic constitutive model for evolving asymmetric/anisotropic hardening behavior of AZ31B and ZEK100 magnesium alloy sheets considering monotonic and reverse loading paths", *Int. J. Plast.* **70** (2015), 30–59.

[Nouailhas et al. 1985] D. Nouailhas, J. L. Chaboche, S. Savalle, and G. Gailletaud, "On the constitutive equations for cyclic plasticity under nonproportional loading", *Int. J. Plast.* **1**:4 (1985), 317–330.

[Ohno 1982] N. Ohno, "A constitutive model of cyclic plasticity with a nonhardening strain region", *J. Appl. Mech.* (*ASME*) **49**:4 (1982), 721–727.

[Qiao et al. 2015] H. Qiao, S. R. Agnew, and P. D. Wu, "Modeling twinning and detwinning behavior of Mg alloy ZK60A during monotonic and cyclic loading", *Int. J. Plast.* **65** (2015), 61–84.

[Rahman et al. 2008] S. M. Rahman, T. Hassan, and E. Corona, "Evaluation of cyclic plasticity models in ratcheting simulation of straight pipes under cyclic bending and steady internal pressure", *Int. J. Plast.* **24**:10 (2008), 1756–1791.

[Smith et al. 2018] B. D. Smith, D. S. Shih, and D. L. McDowell, "Cyclic plasticity experiments and polycrystal plasticity modeling of three distinct Ti alloy microstructures", *Int. J. Plast.* **101** (2018), 1–23.

[Taleb and Cailletaud 2011] L. Taleb and G. Cailletaud, "Cyclic accumulation of the inelastic strain in the 304L SS under stress control at room temperature: ratcheting or creep?", *Int. J. Plast.* **27**:12 (2011), 1936–1958.

[Taleb et al. 2014] L. Taleb, G. Cailletaud, and K. Saï, "Experimental and numerical analysis about the cyclic behavior of the 304L and 316L stainless steels at 350 °C", *Int. J. Plast.* **61** (2014), 32–48.

[Volkov and Igumnov 2007] I. A. Volkov and L. A. Igumnov, Введение в континуалную механику поврежденной среды, Fizmatlit, Moscow, 2007.

[Volkov and Korotkikh 2008] I. A. Volkov and J. G. Korotkikh, Уравнения состояния вязкоупругопластических сред с повреждениями, Fizmatlit, Moscow, 2008.

[Volkov et al. 2018] I. A. Volkov, L. A. Igumnov, I. S. Tarasov, D. N. Shishulin, and M. T. Markova, "Моделирование усталостной долговечности поликристаллических конструкционных сплавов при блочном несимметричном малоцикловом накружении [Simulation of the fatigue life of polycrystalline structural alloys with block non-symmetrical low-cycle loading]", *Problemy prochnosti i plastichnosti* **80**:1 (2018), 15–30.

[Yu et al. 2015] C. Yu, G. Kang, D. Song, and Q. Kan, "Effect of martensite reorientation and reorientation-induced plasticity on multiaxial transformation ratchetting of super-elastic NiTi shape memory alloy: new consideration in constitutive model", *Int. J. Plast.* **64** (2015), 69–101.

[Zecevic and Knezevic 2015] M. Zecevic and M. Knezevic, "A dislocation density based elasto-plastic self-consistent model for the prediction of cyclic deformation: application to AA6022-T4", *Int. J. Plast.* **72** (2015), 200–217.

[Zhu et al. 2014] Y. Zhu, G. Kang, Q. Kan, and O. T. Bruhns, "Logarithmic stress rate based constitutive model for cyclic loading in finite plasticity", *Int. J. Plast.* **54** (2014), 34–55.

[Zhu et al. 2017] Y. Zhu, G. Kang, and C. Yu, "A finite cyclic elasto-plastic constitutive model to improve the description of cyclic stress-strain hysteresis loops", *Int. J. Plast.* **95** (2017), 191–215.

Received 2 Sep 2019. Revised 8 Jan 2020. Accepted 20 Feb 2020.

DMITRY ABASHEV: abashev.d@gmail.com
Moscow Polytech, Moscow, 107023, Russia

VALENTIN BONDAR: tm@mospolytech.ru
Moscow Polytech, Moscow, 107023, Russia

JOURNAL OF MECHANICS OF MATERIALS AND STRUCTURES

msp.org/jomms

Founded by Charles R. Steele and Marie-Louise Steele

Cover photo: Mando Gomez, www.mandolux.com

See msp.org/jomms for submission guidelines.

JoMMS (ISSN 1559-3959) at Mathematical Sciences Publishers, 798 Evans Hall #6840, c/o University of California, Berkeley, CA 94720-3840, is published in 10 issues a year. The subscription price for 2020 is US $660/year for the electronic version, and $830/year (+$60, if shipping outside the US) for print and electronic. Subscriptions, requests for back issues, and changes of address should be sent to MSP.

JoMMS peer-review and production is managed by EditFlow® from Mathematical Sciences Publishers.

PUBLISHED BY

mathematical sciences publishers

nonprofit scientific publishing

http://msp.org/

Journal of Mechanics of Materials and Structures

Volume 15, No. 2 March 2020